Editors' Suggestion

Physical mechanisms of the linear stabilization of convection by rotation

Jeffrey R. Carpenter*
Institute for Coastal Ocean Dynamics, Helmholtz-Zentrum Hereon, Geesthacht 21502, Germany

Yu Liang and Mary-Louise Timmermans
Department of Earth and Planetary Sciences, Yale University, New Haven, Connecticut 06520, USA

Eyal Heifetz
Department of Geophysics, Tel Aviv University, Tel Aviv 69978, Israel

(Received 17 January 2022; accepted 6 July 2022; published 4 August 2022)

Despite the well-known limitations of linear stability theory in describing nonlinear and turbulent flows, it has been found to accurately capture the transitions between certain nonlinear flow behavior. Specifically, the transition in heat flux scaling in rotating convective flows can be well predicted by applying a linear stability analysis to simple profiles of a convective boundary layer. This fact motivates the present study of the linear mechanisms involved in the stability properties of simple convective setups subject to rotation. We look at an idealized two-layer setup and gradually add complexity by including rotation, a bounded domain, and viscosity. The two-layer setup has the advantage of allowing for the use of wave interaction theory, traditionally applied to understand stratified and homogeneous shear flow instabilities, in order to quantify the various physical mechanisms leading to the growth of convective instabilities. We quantitatively show that the physical mechanisms involved in the stabilization of convection by rotation take two different forms acting within the stratified interfacial region, and in the homogeneous mixed layers. The latter of these we associate with the tendency of a rotating flow to develop Taylor columns (TCs). This TC mechanism can lead to both a stabilization or destabilization of the instability and varies depending on the parameters of the problem. A simple criterion is found for classifying the influence of these physical mechanisms.

DOI: 10.1103/PhysRevFluids.7.083501

I. INTRODUCTION

This paper provides a different view on understanding the stabilizing effects of planetary rotation on convection. It resulted from discussions of the influence of planetary rotation, i.e., a rotating frame of reference arising from the Earth's rotation, on the flux of heat through oceanic double diffusive staircases. This influence can be well described through the application of linear stability analysis to the diffusive boundary layer of a double diffusive interface [1].

The stabilizing effect of rotation on convection was first studied theoretically by Chandrasekhar [2] and Nakagawa and Frenzen [3] using a linear stability analysis; and by Veronis [4] using a finite-amplitude stability analysis. The authors found that rotation inhibits the onset of convection by increasing the critical Rayleigh number required to initiate instability, which depends on the rotation rate. This was later confirmed in the fully nonlinear regime through the seminal tank experiments of Rossby [5], where the convective heat flux was found to be inhibited in the presence of strong

*jeff.carpenter@hereon.de

 ©2022 American Physical Society

rotation. Later studies focused on the effect of rotation on flow pattern formation [e.g., [6–11]] and heat flux scaling laws [e.g., [11–15]], with a review by Stevens *et al.* [16].

Despite this large body of work devoted to rotating convection, little attention has been given to further elucidating the physical mechanisms of the stabilizing effect of rotation. The most commonly cited physical explanation for the stabilization is a single paragraph in Chandrasekhar [2]. This, however, offers only a qualitative description of the special case of a linearly stratified, vertically bounded, viscous layer of rotating fluid. Such a setup is not generally present in the case of a convective boundary layer (either double diffusive or purely thermal), where a relatively thin gravitationally unstable stratification is bounded on one side with a large expanse of homogeneous fluid in the adjacent mixed layer [e.g., [15,17]].

Here we examine the physical mechanisms responsible for the stabilization of convection by planetary rotation in an idealized model of a convective boundary layer. Our goal is to construct a quantitative analysis of different physical mechanisms that are operating, rather than to present new linear stability results. The focus is on gaining physical insight into the stabilization of convection by rotation. Specifically, by approximating the boundary layer as an infinitely thin interface with a finite change in buoyancy across it, we are able to provide analytical insight to the instability physics that is also qualitatively similar to the full stability analysis (requiring a numerical solution) that was found to accurately describe the heat flux dependence on rotation from a double diffusive interface [1]. It is also a similar configuration to the laboratory study of Baldwin *et al.* [18], where two homogeneous layers of constant buoyancy are separated by a sharp convectively unstable interface and subjected to varying levels of rotation. We start with the simplest setups, adding levels of complexity stepwise, to see how each added feature (rotation, viscosity, a semibounded domain) of the setup affects the stability and the physical mechanisms involved.

To aid in our physical interpretation, we borrow heavily from the wave interaction theory (WIT) that is often used to provide a physical mechanism for various features of shear flow instabilities [e.g., [19,20]] such as the presence of different instability types [21–23], optimal transient growth [24], the general stability conditions [25], and the structure of the eigenvalue spectrum [26]. This technique generally uses the vorticity field and its relation to the vertical velocity and interface displacement fields in order to construct a visual, and mathematical, description of the relevant interacting interfacial waves. Strict application of WIT requires that the flow be described by distinct interfaces, and allows for a quantification of the influence of various mechanisms on the stability of the convection so that the most important effects can be isolated. As we will show, this leads to a different description of the physical mechanisms by which rotation stabilizes convection, and their dependence on various parameters.

The paper is organized as follows. In the following section, we outline the general linear stability problem and the simplifications that arise when a two-layer setup is adopted, as well as a brief introduction to the wave interaction theory. In Sec. III, a number of simple setups are examined when the flow is taken as inviscid. The essential physical mechanisms are described for the simplest case of nonrotating, inviscid convection and its alteration by rotation and by a bounded domain. In Sec. IV, we look at the viscous case, demonstrating that the inviscid mechanisms identified in the previous section carry over. A summary and conclusions are presented in the final section.

II. LINEAR STABILITY ANALYSIS

A. Derivation

A general derivation of the linearized equations, and the linear stability problem, is first derived for the full viscous, rotating, two-layer setup (see Fig. 1 for a visual guide). The basic equilibrium, or background, state consists of a motionless hydrostatic balance with a vertical buoyancy profile specified by $B(z)$. We will neglect diffusion of the buoyancy scalar field throughout, compatible with our two-layer model. This approximation is valid in the case of immiscible fluids (wherein a neglected surface tension between the layers may arise), as well as in the limit of large Prandtl

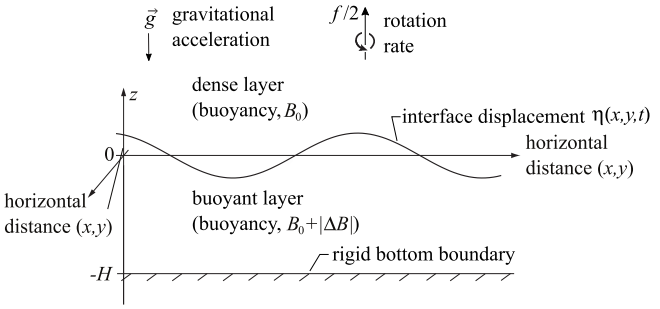

FIG. 1. Sketch of the relevant elements in the two-layer convection setup that is used.

numbers, ν/κ, where ν is the kinematic viscosity and κ the buoyancy diffusivity. The latter can be seen through a nondimensionalization of the equations by ν and a length scale, whereas nondimensionalization by κ and a length scale leads to a different (slow time) limit [27].

The linearized equations of motion for perturbations to this stratified, nondiffusive, Boussinesq fluid from the equilibrium state are

$$u_t - fv = -\pi_x + \nu\nabla^2 u, \tag{1}$$

$$v_t + fu = -\pi_y + \nu\nabla^2 v, \tag{2}$$

$$w_t = -\pi_z + b + \nu\nabla^2 w, \tag{3}$$

in addition to continuity,

$$u_x + v_y + w_z = 0, \tag{4}$$

and buoyancy advection (without diffusion),

$$b_t + wB_z = 0. \tag{5}$$

They consist of (in order) the three components of momentum, continuity, and an advection equation for the buoyancy, $b \equiv -g\rho/\rho_0$, with density perturbations represented by ρ, g the gravitational acceleration, and ρ_0 a representative fluid density. We use a Cartesian coordinate system $\vec{x} = (x, y, z)$ with z the vertical coordinate, opposing g, with velocities $\vec{u} = (u, v, w)$. Other variables used are time t, a density-scaled pressure $\pi \equiv p/\rho_0$, with pressure p, and f which is twice the local vertical rotation rate, commonly called the Coriolis frequency. Subscripts denote partial differentiation. The only equilibrium (also called basic state or background) variable to appear in the equations is the vertical gradient of the buoyancy profile $B_z(z)$, and all other quantities represent a perturbation from the equilibrium.

It is helpful to immediately simplify these equations by first taking the divergence of the momentum equations to give

$$-f\zeta = -\nabla^2\pi + b_z,$$

and to substitute this into the Laplacian of the vertical momentum equation to eliminate the scaled pressure,

$$\frac{\partial}{\partial t}\nabla^2 w = -f\zeta_z + \nabla_H^2 b + \nu\nabla^4 w. \tag{6}$$

Here we have defined the vertical relative vorticity (perturbation) as $\zeta \equiv v_x - u_y$, and the horizontal Laplacian $\nabla_H^2 \equiv \partial^2/\partial x^2 + \partial^2/\partial y^2$. Second, the curl of the horizontal momentum equations can be

taken to give

$$\zeta_t - f w_z = \nu \nabla^2 \zeta. \tag{7}$$

These steps have reduced the equation set to three equations [(6), (7), and (5)] in the three variables $\{w, \zeta, b\}$.

In order to make analytical progress, we take all perturbation quantities to be represented by the normal mode form, as in $w(x, y, z, t) = \hat{w}(z) e^{\sigma t + i(kx + \ell y)}$ for the vertical velocity, with the real part of this expression implicitly intended. We can then write our equation set as

$$(\sigma - \nu L) L(\hat{w}) = -f \hat{\zeta}' - \tilde{k}^2 \hat{b}, \tag{8}$$

$$(\sigma - \nu L) \hat{\zeta} = f \hat{w}', \tag{9}$$

$$\sigma \hat{b} = -B_z \hat{w}, \tag{10}$$

where we have defined the operator $L \equiv d^2/dz^2 - \tilde{k}^2$, with $\tilde{k}^2 \equiv k^2 + \ell^2$ the squared amplitude of the wave-number vector, $\vec{k} = (k, \ell)$. For all hatted normal mode variables, the primes denote ordinary differentiation with respect to z. It is possible to eliminate $\hat{b}$,

$$\sigma(\sigma - \nu L) L(\hat{w}) = -\sigma f \hat{\zeta}' + \tilde{k}^2 B_z \hat{w}, \tag{11}$$

which can be combined with a differentiated (9) to give a single equation for $\hat{w}$ of

$$\sigma(\sigma - \nu L)^2 L(\hat{w}) + \sigma f^2 \hat{w}'' = \tilde{k}^2 (\sigma - \nu L)(B_z \hat{w}). \tag{12}$$

In the following sections, we will consider solutions to this equation, and various simplifications thereof. In addition, we will apply the boundary conditions

$$\hat{w} = 0 \quad \text{at } z = +\infty,\ z_b \tag{13}$$

in all variations of the setup. Two choices for the location of the lower boundary will be examined, $z_b \in \{-\infty, -H\}$, corresponding to infinite and semi-infinite (bounded from below) domains, respectively.

B. Two-layer formulation

We simplify (12) immediately by substituting in our two-layer background the buoyancy profile with $B_z = -|\Delta B| \delta(z)$, where $\delta(z)$ is the Dirac delta function, and $\Delta B < 0$ the buoyancy difference across the layers for a convectively unstable profile. This splits the problem up into one for the layers (i.e., where $z \neq 0$) and one for the interface (at $z = 0$) since in the layers we have eliminated the right-hand side of (12), so

$$(\sigma - \nu L)^2 L(\hat{w}) + f^2 \hat{w}'' = 0. \tag{14}$$

At the interface, the δ function singularity on the right-hand side of (12) requires that we integrate across the interface and apply a series of "jump" conditions on the solution across it [see, e.g., [20]]. These correspond to the following physical principles, with the interfacial jump denoted $[\![X]\!]_0 \equiv X(0^+) - X(0^-)$:

(i) Continuity in vertical velocity: $[\![\hat{w}]\!]_0 = 0$.

(ii) Continuity in vertical stress, which can be expressed as $[\![\hat{\pi}]\!]_0 = 0$. However, in practice, this condition is not explicitly used. Instead, we integrate (12) across the interface in each case. The Appendix describes the equivalence of these two approaches.

(iii) Continuity in horizontal velocity (for viscous flows): $[\![\hat{u}]\!]_0 = 0$ and $[\![\hat{v}]\!]_0 = 0$ implies $[\![\hat{w}']\!]_0 = 0$.

(iv) Continuity in horizontal stress (for viscous flows, see [28]): $[\![\hat{u}' + ik\hat{w}]\!]_0 = 0$ and $[\![\hat{v}' + i\ell\hat{w}]\!]_0 = 0$ implies $[\![\hat{w}'']\!]_0 = 0$.

(v) Continuity of vertical vorticity (for viscous, rotating flows): $[\![\hat{\zeta}]\!]_0 = 0$. In practice, this condition (and the following one) is used in combination with (9) relating $\hat{w}$ to $\hat{\zeta}$.

(vi) Continuity of the vertical derivative of vertical vorticity (for viscous, rotating flows): $[\![\hat{\zeta}']\!]_0 = 0$.

C. Application of wave interaction theory

To understand the physical mechanism, we will adopt a WIT-type approach, by formulating the interaction between the horizontal vorticity, vertical velocity, and vertical displacement of the buoyancy interface. In past studies, this approach has been used to quantify the interactions between interfaces that support stable wave motions, such as gravitationally stable buoyancy interfaces (supporting internal gravity waves) and vorticity interfaces (supporting interfacial Rossby/vorticity waves) [20,21,25]. Each wave has a vertical velocity field that can affect the growth and propagation of the other wave; thus, when conditions are right, they are able to cause each other to propagate in phase and experience mutual growth. Despite the setup considered herein, namely, that of a single (gravitationally unstable) buoyancy interface, the techniques of WIT are used to quantify how the interface interacts with itself and other sources of vertical velocity (e.g., the presence of a boundary). Describing this self-interaction consists of quantifying the interplay of the vertical velocity, interfacial vorticity, and vertical displacement fields, their relationship to each other, and their relative orientations responsible for instability growth. Note that this self-interaction has also been discussed in the context of stratified shear layer instabilities [23].

For an infinitely thin interface in an inviscid flow, it is not the vorticity, but rather the vortex sheet strength that is relevant. The sheet strength is defined as the integrated horizontal vorticity perturbation across the interface, i.e.,

$$\vec{\gamma} \equiv \int_{0^-}^{0^+} \vec{q}_H \, dz \;\Rightarrow\; \vec{\hat{\gamma}} = (-[\![\hat{v}]\!]_0, [\![\hat{u}]\!]_0, 0).$$

Here we use $\vec{q}_H \equiv (w_y - v_z, u_z - w_x, 0)$, and the last expression is the normal mode form of the sheet strength. However, we will often refer to $\vec{\gamma}$ as the "interfacial vorticity" since it is less cumbersome than the "interfacial vortex sheet strength."

Using the horizontal momentum equations in (1)–(3), we can derive a modal interfacial vorticity equation, namely,

$$\sigma \vec{\hat{\gamma}} = f \vec{\hat{\gamma}}_\perp + i|\Delta B| \hat{\eta} \vec{k}_\perp. \tag{15}$$

Here we have denoted the vertical displacement of the interface as η, and used the normal mode form of the relation, $b = -B_z \eta$, given by $\hat{b} = |\Delta B| \delta(z) \hat{\eta}$. In addition, we have defined the perpendicular vector to $\vec{X} = (X_1, X_2)$ as $\vec{X}_\perp \equiv (X_2, -X_1)$, and have neglected the viscous term since viscosity eliminates the vortex sheet at the interface. The physical meaning of the various terms in this equation will be discussed throughout the text below.

The last mathematical tool that we will need in our physical interpretation is to understand the effect that the interfacial vorticity distribution has on the vertical velocity. Once this is known, we can directly assess the changes in interface displacement through the linearised kinematic condition,

$$\frac{D\eta}{Dt} = w \;\Rightarrow\; \sigma \hat{\eta} = \hat{w}(0). \tag{16}$$

The relationship between the interfacial vorticity and the vertical velocity at the interface must be found in each particular setup considered, as is outlined below.

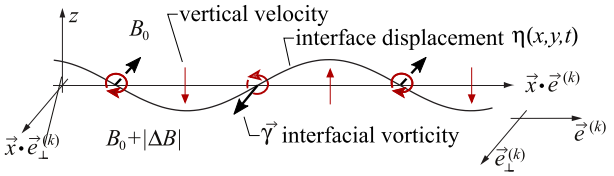

FIG. 2. Schematic of the growth of a convectively unstable interface in a nonrotating frame. The red color is chosen to highlight the relationship between interfacial vorticity and vertical velocity at the interface; they are $\pi/2$ radians out of phase such that upwards (downwards) velocities are present in crests (troughs) of the interface displacement, inducing a growth of the interface.

III. INVISCID SOLUTIONS AND THEIR PHYSICAL MECHANISMS

A. Inviscid, unbounded, nonrotating convective instability

We begin with the simplest case of an inviscid, unbounded, nonrotating two-layer setup, as discussed in Smyth and Carpenter [20]. The equation governing the mixed layers is found by setting $\nu = f = 0$ in (14), i.e., $L(\hat{w}) = 0$. Note that this equation is simply an expression of the fact that in this case, the mixed layers are irrotational since $L(\hat{w})$ is closely related to the horizontal vorticity through $L(\hat{w}) = i\vec{k}_\perp \cdot \vec{\hat{q}}_H$. A simple solution can be found taking $\hat{w}(z) = Ae^{-\tilde{k}|z|}$, with A an arbitrary constant amplitude. Here we have applied both jump condition (i) and the boundary conditions (13). The dispersion relation for the growth rate is then found using jump condition (ii), obtained by integrating (12) with $\nu = f = 0$ across the interface, giving

$$\sigma^2 [\![\hat{w}']\!]_0 + \tilde{k}^2 |\Delta B| \hat{w}(0) = 0, \tag{17}$$

and substituting for $\hat{w}(z)$, finally,

$$\sigma = \pm \left(\frac{|\Delta B| \tilde{k}}{2} \right)^{1/2}, \tag{18}$$

as in [20,29].

A couple of features of this solution are worth noting. First, the entire range of $\tilde{k}$ has an unstable (convective) mode and the growth rate increases with increasing $\tilde{k}$, as well as the buoyancy forcing $|\Delta B|$. This situation is often referred to as an ultraviolet catastrophe, and, as will be seen, is not realistic in viscous fluids. Second, the spatial decay of the vertical velocity away from the interface has a length scale proportional to $\tilde{k}^{-1}$. This is a very general result of motion in an unbounded layer of fluid that is irrotational. The same result is also found in, for example, the depth dependence of ocean surface waves in deep water [30] or in interfacial Rossby waves (also called vorticity waves) in shear flows [31,32].

Physical mechanism

The growth of the instability can be understood physically through a consideration of the interfacial vorticity equation (15), which in this case reduces to

$$\sigma \vec{\hat{\gamma}} = i|\Delta B| \hat{\eta} \vec{k}_\perp. \tag{19}$$

This describes the unsteady growth of interfacial vorticity (left-hand side, lhs) through the baroclinic production (rhs) that arises from any horizontal gradients in buoyancy. The interfacial vorticity generation is proportional to the buoyancy jump and is strongest at the nodes of the displacement (due to the i that is present, which causes a $\pi/2$ phase shift;, see Fig. 2) where slopes, $\tilde{k}\hat{\eta}$, are strongest. The relationship between the displacement and the interface vorticity is sketched in Fig. 2, where we also note that the generation of interfacial vorticity is in the direction of $\vec{k}_\perp$.

To understand the effect that this interfacial vorticity distribution has on the growth of the interface displacement [through the kinematic condition in (16)], we quantify the connection to the vertical velocity at the interface, $\hat{w}(0)$. This can be done by using the definition of $\vec{\hat{\gamma}}$ and its component in the $\vec{k}_\perp$ direction, to give

$$\vec{\hat{\gamma}} \cdot \vec{k}_\perp = -i[\![\hat{w}']\!]_0. \tag{20}$$

Substituting from the solution for $\hat{w}$, this produces the result that $i\vec{\hat{\gamma}} \cdot \vec{k}_\perp = -2\tilde{k}\hat{w}(0)$, which allows us to solve for the vertical velocity at the interface,

$$\hat{w}(0) = -\frac{i}{2}\vec{\hat{\gamma}} \cdot \vec{e}_\perp^{(k)}, \tag{21}$$

where $\vec{e}_\perp^{(k)}$ denotes the unit vector in the $\vec{k}_\perp$ direction. This is an important result that shows it is the component of the interfacial vorticity that is perpendicular to $\vec{k}$ that is responsible for generating vertical velocity at the interface. If, for whatever reason, the interfacial vorticity were oriented entirely along $\vec{e}^{(k)}$, then no vertical velocity would be produced. However, in the present case, $\vec{\hat{\gamma}}$ is oriented in the optimal configuration along $\vec{e}_\perp^{(k)}$. This can be verified by taking the dot product of (19) with $\vec{k}$. Also note that the dispersion relation can be recovered by taking the dot product of (19) with $\vec{k}_\perp$, multiplying by σ, and substituting both the kinematic condition and (21).

In summary, we can construct the following chain of events to understand the growth of the interface displacement (and other fields), with reference to Fig. 2. A small perturbation of the interface with wave-number vector $\vec{k}$ will generate interfacial baroclinic vorticity that is maximum at the nodes of the displacement, and in the direction of $\vec{k}_\perp$. In this optimum orientation, the interfacial vorticity produces a vertical velocity that is in phase with the interface displacement, and thus the displacement grows, creating a positive feedback between displacement, interfacial vorticity, and vertical velocity. Although this physical explanation is considerably more indirect than the much more common "heavy fluid tends to fall and lighter fluid tends to rise" approach, it will be helpful in subsequent sections when quantifying the effects of rotation and boundaries. A similar physical explanation has been described previously by Roberts and Jacobs [33].

B. Inviscid, unbounded, rotating convective instability

By now adding rotation while maintaining an inviscid, unbounded setup, we seek solutions for (14) with $\nu = 0$, i.e.,

$$\sigma^2 L(\hat{w}) + f^2 \hat{w}'' = 0. \tag{22}$$

These take the form of $\hat{w}(z) \propto e^{rz}$, leading to a characteristic equation for the inverse length scale, r, with solutions of

$$r = \pm \frac{\sigma}{(\sigma^2 + f^2)^{1/2}} \tilde{k}.$$

By defining the dimensionless growth rate as $\sigma_* \equiv \sigma/f$, this can be written as

$$r = \pm \frac{\sigma_*}{(\sigma_*^2 + 1)^{1/2}} \tilde{k}.$$

We now choose the correct sign of r to satisfy the boundary conditions that w should vanish as $|z| \to \infty$ to give $\hat{w}(z) = Ae^{-r|z|}$, with r taken positive from now on. Note that there are two regimes of r: (i) $r \sim \sigma_* \tilde{k}$ for $\sigma_* \ll 1$ so that for conditions where rotation dominates the growth rate (i.e., small σ_*), we recover "Taylor column"-like behavior, where the vertical velocity extends far beyond the interface level, and (ii) $r \sim \tilde{k}$ for $\sigma_* \gg 1$ to give the standard exponential decay with a wave number that is present in the nonrotating case.

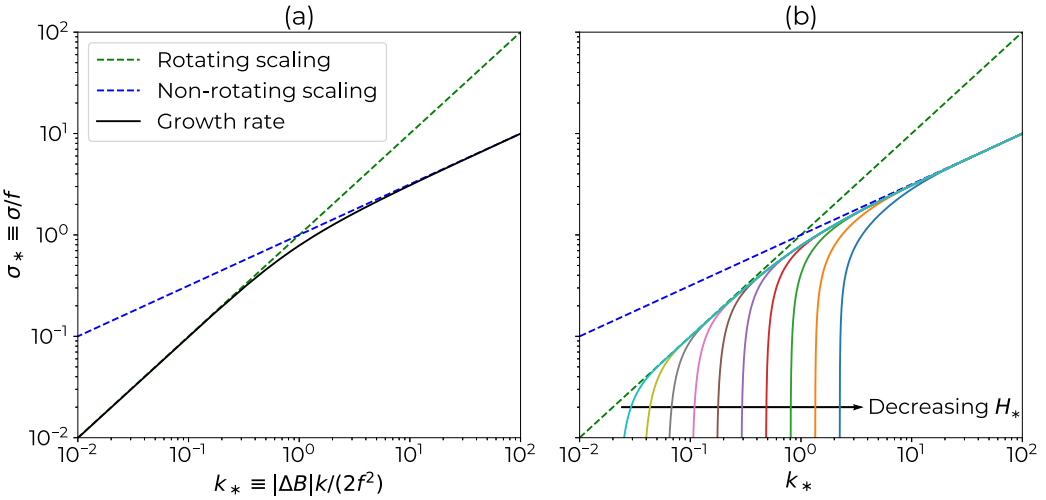

FIG. 3. (a) Plot of the dispersion relation for inviscid, unbounded, rotating convection in the two-layer setup. (b) The effects of including a boundary at a dimensionless distance of $H_* \equiv H/L_R$ from the interface. The different colored solid curves in (b) represent growth rates at differing values of H_*. The dashed curves in both panels are the rotating and nonrotating scalings.

The dispersion relation is found through jump condition (ii) by integrating across the interface, to give

$$(\sigma^2 + f^2)[\![\hat{w}']\!]_0 - \tilde{k}^2 \Delta B \hat{w}(0) = 0. \tag{23}$$

Substituting in our solution above, we find the following dimensional equation for the growth rate:

$$\sigma(\sigma^2 + f^2)^{1/2} + \frac{\Delta B \tilde{k}}{2} = 0,$$

in agreement with Chandrasekhar [29]. This can be written in dimensionless form as

$$\sigma_*(\sigma_*^2 + 1)^{1/2} - k_* = 0, \tag{24}$$

where $k_* = L_R \tilde{k}$ with $L_R \equiv |\Delta B|/(2f^2)$ a length scale. Note that k_* can be thought of as the square of the ratio of two inverse timescales: the buoyant growth rate $\sigma_{\text{buoy}} \equiv (|\Delta B|\tilde{k}/2)^{1/2}$ and the Coriolis frequency f, with $k_* = (\sigma_{\text{buoy}}/f)^2$. There are again two limits: (i) $\sigma_* \ll 1$ so that rotation is dominant and $\sigma_* \sim k_*$, and (ii) $\sigma_* \gg 1$ so that rotation is negligible and $\sigma_* \sim k_*^{1/2}$, just as in the case where $f = 0$ above. These two regimes can be seen in the solution of the full dispersion relation shown in Fig. 3(a), with a transition region centered around $\sigma_* \approx 1$. Note that we can rewrite the limits in terms of the length scale, L_R, based on whether or not $\tilde{k} \gg L_R$ (nonrotating) or $\tilde{k} \ll L_R$ (rotating).

Physical mechanism

It is clear from Fig. 3(a) that by including rotation, the growth of the instability has been damped for $\sigma_* \lesssim 1$ (or $k_* \lesssim 1$). We now examine the physical mechanisms behind this damping, which can be seen to arise from two competing effects: (i) a new source of vorticity in the layers that leads to increases in vertical velocity at the interface, and (ii) a misalignment of the interfacial vorticity and $\vec{k}_\perp$ vectors that arises from rotation effects within the interface, and leads to reduced vertical velocities. Each effect is examined in turn and referenced to the various processes sketched in the visual aid of Fig. 4.

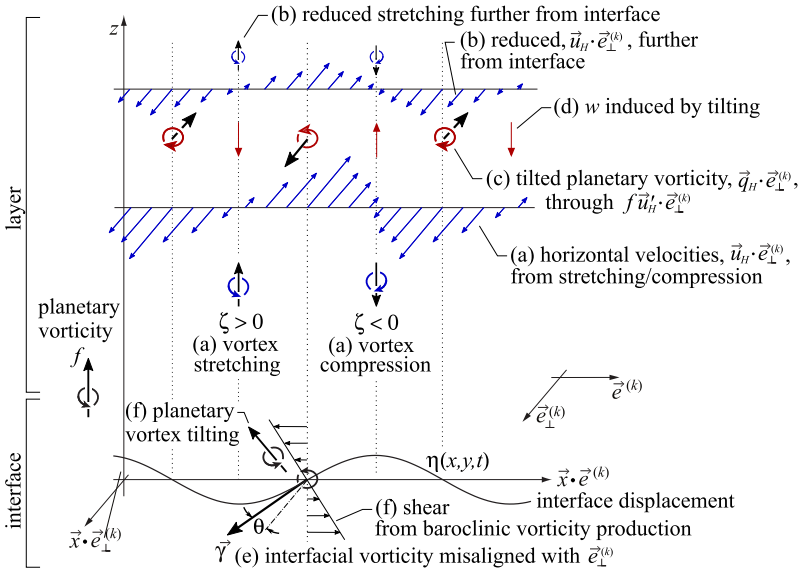

FIG. 4. Illustration of the mechanisms acting in rotating convection that lead to increased vertical velocities at the interface, as well as the misalignment of the interfacial vorticity with the $\vec{k}_\perp$ direction of baroclinic vorticity production. For brevity, only the interface and upper mixed layer are shown. Colors are used to group the vorticity sources with their associated velocities.

Layer mechanism. New sources and sinks of perturbation vorticity must be considered in a rotating frame of reference due to the presence of planetary vorticity, f. This effect manifests itself first, in the layers, through a stretching/compression of the (vertical) planetary vorticity term, i.e., $f\hat{w}'$ in (9), rewritten here for convenience,

$$\sigma\hat{\zeta} = f\hat{w}'.$$

This equation describes the production of vertical vorticity in the layers due to vertical gradients in vertical velocity leading to stretching/compression of planetary vorticity, f. A sketch of this process is shown in Figs. 4(a) and 4(b); in the crests (troughs) of the interface displacement, there is a compression (stretching) of planetary vorticity. This results in horizontal velocities in the layers [Fig. 4(a)]. Due to the decay of $\hat{w}(z)$ away from the interface (i.e., such that $\hat{w}'' \neq 0$), vertical gradients of $\hat{\zeta}$ are present in the layers. This has important consequences because it leads to the production of horizontal vorticity in the layers through (11), modified for this particular case to

$$\sigma L(\hat{w}) = -f\hat{\zeta}' \tag{25}$$

in the layers. To see this, we substitute the following relations involving the horizontal (layer) vorticity $i\tilde{k}\vec{\hat{q}}_H \cdot \vec{e}_\perp^{(k)} = L(\hat{w})$, and the vertical vorticity $\hat{\zeta} = -i\tilde{k}\vec{\hat{u}}_H \cdot \vec{e}_\perp^{(k)}$. This results in a rewritten (25), namely,

$$\sigma\vec{\hat{q}}_H \cdot \vec{e}_\perp^{(k)} = f\vec{\hat{u}}_H' \cdot \vec{e}_\perp^{(k)}, \tag{26}$$

showing that horizontal vorticity is generated in the $\vec{k}_\perp$ direction through the tilting of vertical planetary vorticity by the vertical shear. This vertical shear arises due to the horizontal velocities (along $\vec{k}_\perp$) that accompany the stretching/compression process, as shown schematically in Fig. 4(c). It is the phase of the produced horizontal vorticity that leads to upwards (downwards) velocities at crests (troughs) of the displacement field, which, acting alone, causes an increase in the vertical velocity compared to the nonrotating case [Fig. 4(d)].

The increase in vertical velocity at the interface arising from vortex tilting in the layers can be quantified using (20) and, substituting the solution for the rotating case,

$$\vec{\hat{\gamma}}\cdot\vec{k}_\perp = 2ir\hat{w}(0) \;\Rightarrow\; \hat{w}(0) = -\frac{i}{2}\vec{\hat{\gamma}}\cdot\vec{e}_\perp^{(k)}(1+\sigma_*^{-2})^{1/2}. \tag{27}$$

Thus, by comparing to (21), we see that the vertical velocity at the interface is increased by the factor $(1+\sigma_*^{-2})^{1/2}$ above the nonrotating case. Acting alone, rotation would then lead to an *increase* in growth rate above the nonrotating case, which is not found. The reason is due to the action of the interfacial vorticity, which we now describe.

Interface mechanism. From inspection of the interfacial vorticity equation (15), we can see that vorticity is produced by the baroclinic term in the direction of $\vec{k}_\perp$, while the effect of rotation (in the term $f\vec{\hat{\gamma}}_\perp$) is to rotate the vorticity vector away from this direction. The angle θ that $\vec{\hat{\gamma}}$ makes with the direction of the baroclinic source term along $\vec{k}_\perp$ can be found through taking $\cdot\,\vec{e}^{(k)}$ of (15). We find that $\vec{\hat{\gamma}}$ is perpendicular to $\sigma\vec{e}^{(k)} + f\vec{e}_\perp^{(k)}$, and the angle that it departs from $\vec{k}_\perp$ is

$$\theta = \tan^{-1}(\sigma_*^{-1}),$$

as sketched in Fig. 4(e). This shows that for conditions where rotation is dominating the growth rate, $\sigma_* \ll 1$ and $\theta \to \pi/2$ so that $\vec{\hat{\gamma}}$ is aligned with $\vec{k}$. Therefore, rotation shifts $\vec{\hat{\gamma}}$ to a position where it generates a reduced vertical velocity at the interface level, via (27). On the other hand, as we saw in the nonrotating case, when buoyancy-driven growth dominates rotation, $\sigma_* \gg 1$, $\theta \to 0$, and $\vec{\hat{\gamma}}$ is closely aligned with the baroclinic forcing direction, along $\vec{k}_\perp$. The source of this rotationally driven misalignment of $\vec{\hat{\gamma}}$ from the baroclinic forcing direction of $\vec{k}_\perp$ can be seen to arise from the vortex tilting process that is occurring at the interface [Fig. 4(f)]. This comes directly from the definition of $\vec{\hat{\gamma}}_\perp \equiv (\llbracket\hat{u}\rrbracket_0, \llbracket\hat{v}\rrbracket_0, 0)$, so that the term $f\vec{\hat{\gamma}}_\perp$ describes the tilting of planetary vorticity integrated across the interface.

The final reduction in growth rates from the effects of rotation can be seen by comparing the relative magnitudes of the layer- and interface-based vorticity mechanisms described above. This can be done by writing the interfacial vorticity equation (15) into components that are in the basis $\{\vec{e}^{(k)}, \vec{e}_\perp^{(k)}\}$, and substituting the $\vec{e}^{(k)}$ equation into that for $\vec{e}_\perp^{(k)}$, giving

$$(1+\sigma_*^{-2})\sigma^2\vec{\hat{\gamma}}\cdot\vec{k}_\perp = i|\Delta B|\tilde{k}\hat{w}(0).$$

We can then compare this directly to the nonrotating counterpart, found by multiplying (19) by σ and using the kinematic condition $\sigma\hat{\eta} = \hat{w}(0)$, to give

$$\sigma^2\vec{\hat{\gamma}}\cdot\vec{k}_\perp = i|\Delta B|\tilde{k}\hat{w}(0).$$

Thus, the misalignment in the interfacial vorticity equation due to rotation causes a factor $1+\sigma_*^{-2}$ reduction in the effective vorticity (in the $\vec{e}_\perp^{(k)}$ direction), which can be directly compared to an increase in vertical velocity due to the layer-based mechanism by the factor $(1+\sigma_*^{-2})^{1/2}$. Overall growth rates are therefore reduced by rotation effects, as seen in Fig. 3(a).

We also provide a heuristic interpretation of this interface mechanism that does not appeal to the methods of wave interaction theory in the Appendix.

C. Inviscid, bounded, rotating convective instability

By placing a solid boundary a distance H, below the interface, it is possible to introduce an explicit length scale into the problem. This is an idealization to a convective boundary layer in which both a solid boundary condition and length scale are present. A solution for $\hat{w}(z)$ can immediately be written, once it is recognized that the boundary condition of $\hat{w}(-H) = 0$ can be satisfied by using the method of images [34]. An identical interface is placed equidistant from the boundary

with opposite strength, i.e., the solution takes the form

$$\hat{w}(z) = A(e^{-r|z|} - e^{-r|z+2H|}) \quad \text{for } z \geqslant -H.$$

The resulting dispersion relation is found through the jump condition in (23), which is altered only in the value of the vertical velocity at the interface level, $\hat{w}(0)$, giving

$$\sigma_*(\sigma_*^2 + 1)^{1/2}\mathcal{F}(\sigma_*, k_*, H_*) - k_* = 0. \tag{28}$$

Here we have defined the dimensionless distance to the boundary as $H_* \equiv H/L_R$, and the function

$$\mathcal{F}(\sigma_*, k_*, H_*) \equiv \frac{1}{2}\left\{1 + \coth\left[k_* H_* \frac{\sigma_*}{(\sigma_*^2 + 1)^{1/2}}\right]\right\}.$$

It is worth comparing (28) with the dispersion relation found above in (24) without a boundary. They differ only in how $\mathcal{F}$ differs from unity. Since $\coth(x) \to 1$ as $x \to \infty$, we recover the unbounded case when H_* becomes large (with the other variables held fixed). The results are plotted as a series of curves for different values of H_*, shown in Fig. 3(b). The presence of a boundary provides a complete stabilization of the lowest wave numbers, but otherwise does not alter the growth rates away from the low-k_* cutoff. For fixed values of f and $|\Delta B|$ (and therefore L_R), as the boundary is moved closer to the interface, shorter and shorter wavelengths are stabilized. This can be seen in Fig. 3(b) as the relatively sharp cutoff in growth rate shifts to larger k_* as H_* decreases.

It may appear that the rotational regime can be completely eliminated by a boundary that is sufficiently close. In this scenario, the lowest wave numbers are stabilized before a transition to the rotational scaling regime is reached. However, the location of the cutoff wave number can be found by taking the limit $\sigma_* \to 0^+$ of the dispersion relation, and solving to give $k_*^c = (2H_*)^{-1/2}$. Note that this limit is not independent of rotation, and the rotational regime (i.e., $\sigma_* < 1$) must be crossed to reach stabilization due to the boundary. This can be compared to the nonrotating, bounded case, where there is an exponential decrease in the growth rate with $\sigma_* = k_*^{1/2}(1 - e^{-2k_*H_*})^{1/2}$ versus the unbounded result of $\sigma_* = k_*^{1/2}$ from (18).

Physical mechanism

The stabilization of the convective instability by the proximity of the boundary has a simple physical explanation. As was apparent from the mathematical analysis, the presence of the boundary altered the vertical velocities with the inclusion of the image source. This image has the effect of reducing vertical velocities at the interface level, which in turn reduces the growth of the instability directly through the kinematic condition, $\sigma\hat{\eta} = \hat{w}(0)$. Therefore, for a given interface displacement ($\hat{\eta}$), there will be a lower growth rate (σ) associated with the reduced vertical velocity at the interface. In addition, as the boundary is moved closer to the interface, so too is the image source, thus resulting in a stronger stabilization due to the monotonically increasing vertical velocities with distance to the source. This effect will be more pronounced with increasing rotation rates (decreasing σ_*) due to the reduced vertical decay of $\hat{w}$.

We note that the mechanism identified in the previous section, consisting of horizontal vorticity production in the layers through tilting, and its reinforcing of the vertical velocity field, leads to the reduced vertical decay of $\hat{w}(z)$ from the interface. It may be interpreted as the mechanism for the formation of a flow with vertical "rigidity," which in the strongly rotating limit gives rise to a Taylor-column (TC) structure with vanishing $\hat{w}'(z)$. Although we showed that this mechanism will lead to increased $\hat{w}$ at the interface in the case of an unbounded flow, this is not necessarily the case in a bounded flow since $\hat{w}$ must vanish at the boundary. The influence that each of these two processes has on the convection can be quantified by solving for $\hat{w}(0)$, as done previously:

$$\hat{w}(0) = -\frac{i}{2}\vec{\hat{\gamma}}\cdot\vec{e}_\perp^{(k)}(1 + \sigma_*^{-2})^{1/2}\left\{1 - \exp\left[-2\tilde{k}H\frac{\sigma_*}{(\sigma_*^2 + 1)^{1/2}}\right]\right\}.$$

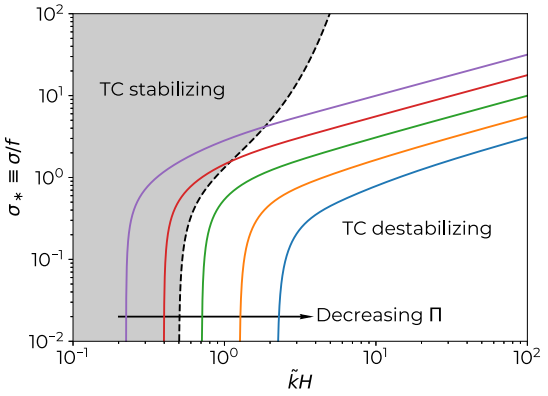

FIG. 5. Growth rates in bounded rotating convection using an alternate nondimensionalization with H as the length scale. The different colored curves represent growth rates at differing values of $\Pi \equiv |\Delta B|/(2f^2H) = (0.100, 0.316, 1.00, 3.16, 10.0)$. The gray region corresponds to conditions where the Taylor-column (TC) effect leads to a stabilization of convection, with destabilized convection at larger $\tilde{k}H$ outside.

Here we see that the presence of a boundary modifies the equivalent unbounded expression in (27) by the factor in the curly braces [35] and online, i.e., $\hat{w}(0)_{\text{bounded}} = \hat{w}(0)_{\text{unbounded}}(1 - e^{-2rH})$.

Therefore, there are two competing effects that we will group together into a Taylor-column (TC) mechanism: (I) layer-based tilting of planetary vorticity that results in an increased $\hat{w}(0)$ and is destabilizing (when acting alone), and (II) the need to satisfy the boundary condition of $\hat{w}(-H) = 0$ which reduces the $\hat{w}(0)$ and stabilizes the convection. These two processes are related: since (I) results in less decay of the image source with vertical distance, it will have larger amplitudes at the interface. Hence the boundary has a greater influence on the growth of the interface through (II). Whether the TC mechanism is leading to an increased or decreased vertical velocity at the interface, and therefore is either helping or hindering the growth of the interface displacement in the presence of a boundary, depends on whether

$$(1 + \sigma_*^{-2})^{1/2}\left\{1 - \exp\left[-2\tilde{k}H\frac{\sigma_*}{(\sigma_*^2 + 1)^{1/2}}\right]\right\} \lessgtr 1.$$

This can be rearranged to yield a condition for the stabilizing effect of the TC mechanism,

$$\tilde{k}H < -\frac{(\sigma_*^2 + 1)^{1/2}}{2\sigma_*}\ln\left[1 - \frac{\sigma_*}{(\sigma_*^2 + 1)^{1/2}}\right]. \tag{29}$$

Waves that are longer than this condition ($\tilde{k}H$ smaller) have layer vorticity that stabilizes the growth of the interface, whereas shorter waves ($\tilde{k}H$ larger) destabilize. This condition is plotted in gray in Fig. 5, where it is now convenient to nondimensionalize using H as the independent length scale with $\tilde{k}H$ the nondimensional wave number. This nondimensionalization results in the dependence of $\sigma_* \equiv \sigma/f$ on the parameter $\Pi \equiv |\Delta B|/(2f^2H)$, rather than experiencing a collapse as in Fig. 3(b). Note that as the convection stabilizes asymptotically with $\sigma_* \to 0^+$, neither of (I) or (II) dominates; rather, (I) increases $\hat{w}(0)$ as rapidly as (II) decreases $\hat{w}(0)$ (with other quantities held fixed) such that their product is constant. This results in the TC stabilization boundary (dashed line separating the gray region in Fig. 5) approaching a constant limit $\tilde{k}H = 1/2$ as $\sigma_* \to 0^+$. Therefore, we find that whether the TC mechanism is stabilizing or destabilizing depends on if Π can be large enough for long waves to penetrate into the gray region with $\tilde{k}H < 1/2$. This occurs for values of $\Pi \gtrsim 2$, which is a simple condition for assessing the potential role of the TC mechanism.

IV. THE EFFECTS OF VISCOSITY

In this section, we now include the viscous terms in the mixed layer differential equation (14), while considering only unbounded domains. This is a sixth-order ordinary differential eigenvalue problem for $\{\sigma, \hat{w}(z)\}$, and we can take eigenfunction solutions of the form $\hat{w}(z) \propto e^{rz}$, resulting in a characteristic equation for $R \equiv r^2$ that is cubic with

$$a_3 R^3 + a_2 R^2 + a_1 R + a_0 = 0, \tag{30}$$

and coefficients given by

$$a_3 = \nu^2, \tag{31}$$

$$a_2 = -(2\sigma\nu + 3\nu^2\tilde{k}^2), \tag{32}$$

$$a_1 = \sigma^2 + 4\sigma\nu\tilde{k}^2 + 3\nu^2\tilde{k}^4 + f^2, \tag{33}$$

$$a_0 = -(\sigma^2\tilde{k}^2 + 2\sigma\nu\tilde{k}^4 + \nu^2\tilde{k}^6). \tag{34}$$

It is helpful to nondimensionalize using the inverse timescale $\nu\tilde{k}^2$, and defining $R_* \equiv R/\tilde{k}^2$ to give

$$a_3^* R_*^3 + a_2^* R_*^2 + a_1^* R_* + a_0^* = 0, \tag{35}$$

with coefficients given by

$$a_3^* = 1, \tag{36}$$

$$a_2^* = -(2\sigma_* + 3), \tag{37}$$

$$a_1^* = \sigma_*^2 + 4\sigma_* + 3 + \tilde{\mathrm{Ek}}^{-2}, \tag{38}$$

$$a_0^* = -(\sigma_*^2 + 2\sigma_* + 1), \tag{39}$$

after dividing by $\nu^2\tilde{k}^6$. Here we have also defined $\sigma_* \equiv \sigma/(\nu\tilde{k}^2)$ and a dimensionless number that has a similar form to an Ekman number, $\tilde{\mathrm{Ek}} \equiv (\nu\tilde{k}^2)/f$. Note that this definition of the dimensionless growth rate, σ_*, differs from that used in the previous section for inviscid flows.

A. Viscous, nonrotating convective instability

The roots of the characteristic equation can easily be found for the nonrotating case with $\tilde{\mathrm{Ek}} = \infty$. These are $R_* = 1$ and the double root $R_* = \sigma_* + 1$. However, through inspection of (11), with the right-hand side equal to zero, we see that one of the two $\sigma_* + 1$ roots is spurious and this results in $r = \pm\tilde{k},\ \pm\sqrt{\sigma_* + 1}\tilde{k}$, with $\hat{w}(z) \propto e^{rz}$ forming a general solution. Most of these solutions can be eliminated based on the boundary conditions that $\hat{w} \to 0$ as $|z| \to \infty$, so the solution is

$$\hat{w}(z) = \begin{cases} A_1 e^{-\tilde{k}z} + A_2 e^{-(\sigma_*+1)^{1/2}\tilde{k}z}, & z > 0 \\ B_1 e^{\tilde{k}z} + B_2 e^{(\sigma_*+1)^{1/2}\tilde{k}z}, & z < 0. \end{cases} \tag{40}$$

We now can solve for the four unknown coefficients using the four jump conditions. The condition for the continuity of vertical stress is equivalent to integrating (11) across the interface, and gives

$$\sigma\nu[\![\hat{w}'''']\!]_0 - \tilde{k}^2|\Delta B|\hat{w}(0) = 0. \tag{41}$$

It is useful to work with the dimensionless form of this jump condition,

$$\sigma_* \frac{[\![\hat{w}'''']\!]_0}{\tilde{k}^3\hat{w}(0)} = \tilde{\mathrm{Ra}},$$

where we have defined a Rayleigh-number-like quantity, $\tilde{\mathrm{Ra}} \equiv |\Delta B|/(\nu^2\tilde{k}^3)$.

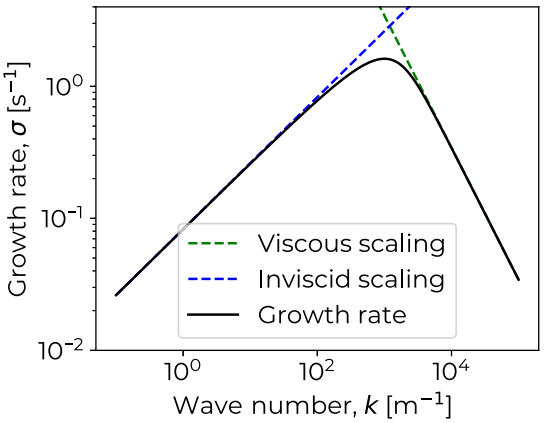

FIG. 6. Plot of the dispersion relation for viscous, nonrotating convection in the two-layer setup. Dimensional parameters are chosen to match the experiments of Davies-Wykes and Dalziel [37], namely, $|\Delta B| = 0.0137\ \mathrm{m\,s^{-2}}$, $\nu = 1.0 \times 10^{-6}\ \mathrm{m^2\,s^{-1}}$. The two asymptotic scalings corresponding to inviscid buoyant growth [i.e., as in (18)], and the viscous damping are shown as the indicated dashed lines.

These four conditions allow us to solve for the four unknown coefficients in (40) and lead to a dispersion relation. In short, we use conditions (i) and (iii) to give $A_2 = B_2$ and, therefore, also $A_1 = B_1$. Then, (ii) results in $A_1 = -(\sigma_* + 1)^{1/2} A_2$ so that the (normalized) solution becomes

$$\hat{w}(z) = e^{-(\sigma_*+1)^{1/2}\tilde{k}|z|} - (\sigma_* + 1)^{1/2} e^{-\tilde{k}|z|}.$$

The dispersion relation reduces to

$$\mathcal{G}(\sigma_*) = \tilde{\mathrm{Ra}} \quad \text{with } \mathcal{G}(\sigma_*) \equiv \frac{2\sigma_*^2(\sigma_* + 1)^{1/2}}{(\sigma_* + 1)^{1/2} - 1},$$

a result previously found by Chandrasekhar [29,36] once the Boussinesq limit is taken. For $\sigma_* \gg 1$, we can identify the inviscid buoyant growth regime, since $\mathcal{G}(\sigma_*) \approx 2\sigma_*^2$, again giving $\sigma = (|\Delta B|\tilde{k}/2)^{1/2}$. On the other hand, the effects of viscosity are felt at low σ_*, and to describe this regime, we expand $\mathcal{G}(\sigma_*)$ about $\sigma_* = 0$ to give $\mathcal{G}(\sigma_*) \approx 4\sigma_*$, so that $\sigma = |\Delta B|/(4\nu\tilde{k})$. This shows that the "roll-off" of σ with $\tilde{k}$ is proportional to $\tilde{k}^{-1}$. It is interesting to note that viscosity does not lead to completely stabilized perturbations at large $\tilde{k}$, as it does for convective systems with thermal variations over a finite vertical domain and nonzero diffusivity [e.g., [20]].

As a specific example, we take the conditions used in the experiments of Davies-Wykes and Dalziel [37], where careful effort was undertaken to produce convection in the two-layer configuration. The results of the stability analysis for this setup are shown in Fig. 6. They show both the inviscid buoyant growth scaling, as well as the viscous roll-off, and this results in a maximum growth wavelength of 0.63 cm. Based on the width of their experimental tank, we would therefore expect to observe approximately 32 developing wavelengths in the initial instability, and this appears to be consistent with their Fig. 5(a) for the initial onset of the instability. However, as they note, this wavelength may be influenced by the initial gate removal.

Physical mechanism

As the growth rate curve follows the inviscid buoyant scaling with a viscous roll-off, the physical mechanism is identical to the inviscid case, but with a wave number of maximum growth set by the onset of viscous damping. This damping is responsible for lower growth rates than would otherwise occur in the absence of viscosity.

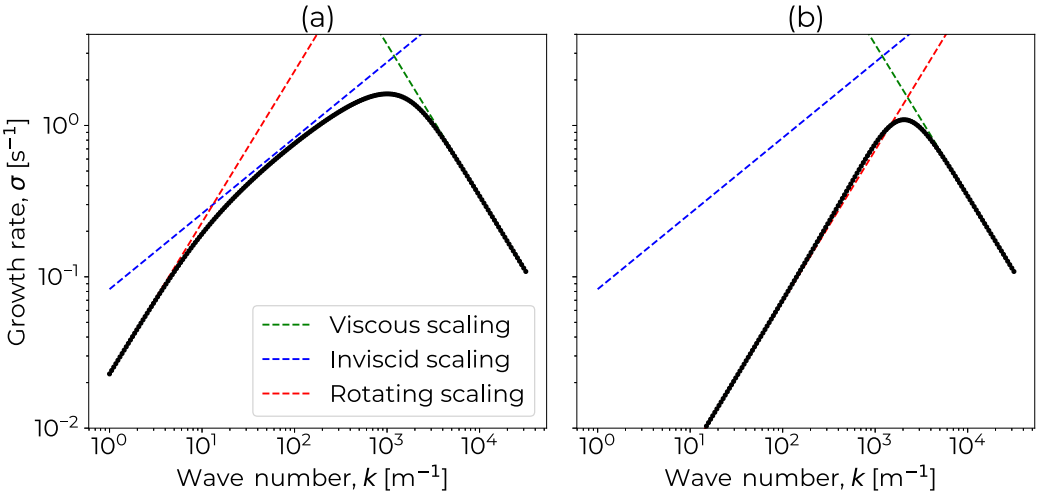

FIG. 7. Plot of the dispersion relation for viscous, rotating convection in the two-layer setup. (a) and (b) correspond to rotation rates of $f = 0.3, 10\ s^{-1}$, respectively. All other dimensional parameters are chosen as in Fig. 6. The three asymptotic scalings corresponding to inviscid buoyant growth [i.e., as in (18)], the viscous roll-off, and rotation-dominated convection are shown as the indicated dashed lines.

B. Viscous, rotating convective instability

By including the rotation term in the cubic equation (35), it can be shown that the roots are no longer purely real; rather, they consist of one real number and two complex conjugate roots. Solutions in the mixed layers then take the form of

$$\hat{w}(z) = \begin{cases} A_1 e^{-r_1 \tilde{k} z} + A_2 e^{-a\tilde{k}z} \cos(b\tilde{k}z) + A_3 e^{-a\tilde{k}z} \sin(b\tilde{k}z), & z > 0 \\ B_1 e^{r_1 \tilde{k} z} + B_2 e^{a\tilde{k}z} \cos(b\tilde{k}z) + B_3 e^{a\tilde{k}z} \sin(b\tilde{k}z), & z < 0, \end{cases} \tag{42}$$

where r_1 denotes the real root, and a and b the real and imaginary parts of the complex conjugate roots, respectively. Note that we have eliminated half of the terms in each layer that have unbounded signs in the exponential function. Unfortunately, we were unable to derive closed-form analytical solutions for the roots, and dispersion relation. These are therefore computed numerically, with example solutions plotted in Fig. 7 for two different rotation rates, f. As far as we are aware, this setup appears to have been solved previously only through approximate methods [38].

The growth rates that result from the viscous, rotating convection setup essentially mirror the individual results from the cases examined so far. Depending on the choice of parameters (i.e., $\tilde{\mathrm{Ra}}$ and $\tilde{\mathrm{Ek}}$), all three scalings can be observed as $\tilde{k}$ is varied: a region at low $\tilde{k}$ where rotation is limiting growth, a region of essentially inviscid buoyant growth at intermediate $\tilde{k}$, and the viscous roll-off at high $\tilde{k}$. All of these regions can be seen in Fig. 7(a). In this case, we note that although rotation alters growth rates, it will not affect the fastest growing mode that is expected to give rise to nonlinear convection. At larger rotation rates (more precisely, smaller $\tilde{\mathrm{Ek}}$), however, the rotating growth scaling moves towards the $\tilde{k}$ of the fastest growing mode, and the stabilizing effects of rotation will be felt during nonlinear convection; $\tilde{k}$ of the fastest growing mode shifts to larger values and growth rates are diminished. The mechanism by which growth rates are reduced is essentially inviscid and follows the same scaling as described in Sec. III B. The mechanism described there also holds for the viscous case, but with viscosity responsible for limiting high $\tilde{k}$ growth, and setting a fastest growing mode. Note that this is in contrast to a linearly stratified, vertically bounded layer of rotating fluid, where viscosity has been found to destabilize convection [2].

V. SUMMARY AND CONCLUSIONS

Stimulated by the close agreement between linear stability results and nonlinear convective heat transports [1], in this paper, we have taken a different look at quantifying the physical mechanisms involved in the linear stabilization of convection by rotation. We do this using an idealized two-layer setup where we add increasing complexity stepwise, i.e., rotation, a semibounded domain, and viscosity. This setup has the advantage of allowing for the quantification of different effects on the growth of the instability using wave interaction theory from the stability of stratified shear flows [25].

Application of this methodology to the inviscid, unbounded, rotating convection problem quantifies two principal effects that contribute to altering the growth rates of convection by rotation: (i) a source of planetary vorticity in the mixed layers that can contribute to an *increase* in growth, that is (ii) more than compensated by *decreasing* growth due to a misalignment of the interfacial vorticity with the interface displacement caused by the tilting of planetary vorticity by interfacial shear. The effect in (i) is related to the development of Taylor columns (TCs) in the layers, and is altered when one of the layers is bounded in the vertical. In this bounded case, the need to satisfy the rigid lid boundary condition causes an additional stabilization, and an approximate condition of $\Pi \equiv |\Delta B|/(2f^2H) > 2$ was developed to determine whether this TC mechanism was acting to stabilize convection. Finally, by including viscosity in the problem, we find, unsurprisingly, that the high wave numbers are stabilized, giving rise to a wave number of maximum growth, $\tilde{k}_{\max}$. However, the mechanisms of stabilization by rotation, and rotational effects on $\tilde{k}_{\max}$, are essentially set by the inviscid mechanisms (i), (ii) discussed above, with viscosity only serving to limit high wave-number growth.

We can therefore summarize the central general result of this study: assessing the physical mechanisms responsible for the linear stabilization of convection by rotation is not straightforward, can be of various types, and depends on the parameters of the problem. For more realistic cases with continuous buoyancy profiles with boundary and mixed layers, the simple setup of a linearly stratified and vertically bounded layer, as in the often-cited paper of Chadrasekhar [2], cannot be used as an idealized guide for a full understanding of the stability mechanisms. A more careful approach is required that accounts for the physical mechanisms identified herein and their dependence on parameters.

ACKNOWLEDGMENTS

Support of J.R.C. by the Helmholtz Association through the PoF-IV programme and through the German Research Foundation (DFG) is gratefully acknowledged. M.L.T. acknowledges support from the National Science Foundation Division of Polar Programs under Award No. 1950077. E.H. is grateful to the Israeli Science Foundation (Grant No. 1645/19) and to the PAZY Foundation (Grant No. 324-2/22). This paper is a contribution to project T2 of the Collaborative Research Centre TRR181, "Energy Transfers in Atmosphere and Ocean" funded through DFG Grant No. 274762653.

APPENDIX A: DERIVATION OF THE CONTINUITY OF VERTICAL STRESS JUMP CONDITION

In this Appendix, we demonstrate that the jump conditions obtained by integrating equation (12) across the singularity at the buoyancy interface are equivalent to requiring a continuous vertical stress. In general, the vertical stress across a horizontal interface is given by $-\pi + 2\nu\partial w/\partial z$ and in normal mode form by $-\hat{\pi} + 2\nu\hat{w}'$. In both the inviscid and viscous cases, the second term vanishes since either $\nu = 0$ or $[\![\hat{w}']\!]_0 = 0$, respectively. Therefore, the continuity of vertical stress across the interface reduces to $[\![\hat{\pi}]\!]_0 = 0$. We now use this condition to recover the jump conditions obtained in the main body of the text by integrating (12) across the interface.

The divergence of the momentum equations in (1)–(3) gives

$$L(\hat{\pi}) = \hat{b}' - f\hat{\zeta}, \tag{A1}$$

which can be used to solve for the pressure by using the Green's function, $G(z, s)$, for the linear operator L, via

$$\hat{\pi}(z) = \int_{-\infty}^{\infty} G(z, s)\hat{F}(s)\, ds, \tag{A2}$$

where $G(z, s) = -e^{-\tilde{k}|z-s|}/2\tilde{k}$ for an unbounded domain, which has been assumed here. The right-hand side of (A1) is represented by $\hat{F}(z)$ and is composed of the vertical derivative of a singular term with $\hat{b} = -B_z\hat{\eta}$ and $B_z = \Delta B\, \delta(z)$. We only consider this singular buoyancy term in $\hat{F}$ since it appears in the jump condition. It is possible to solve for the pressure contribution of this term, which we will denote with the i subscript due to its interfacial jump. It can be written using integration by parts as

$$\hat{\pi}_i(z) = \Delta B \int_{-\infty}^{\infty} \frac{\partial G}{\partial s}\delta(s)\hat{\eta}(s)\, ds, \tag{A3}$$

and results in

$$\hat{\pi}_i(z) = \frac{\Delta B\, \hat{\eta}(0)}{2}\mathrm{sgn}(z)e^{-\tilde{k}|z|}, \tag{A4}$$

giving a jump in pressure across the interface of $[\![\hat{\pi}_i]\!]_0 = \Delta B\, \hat{\eta}(0)$.

In addition to this hydrostatic pressure jump across the interface, there is also a contribution from the layers, which will be denoted with the ℓ subscript. This can be found by taking the horizontal divergence of (1),(2) to find $\hat{\pi}_\ell$ as a function of $\hat{w}$ and $\hat{\zeta}$, i.e.,

$$\hat{\pi}_\ell(z) = \frac{(-\sigma + \nu L)\hat{w}' - f\hat{\zeta}}{\tilde{k}^2}. \tag{A5}$$

Setting the total pressure jump across the interface to zero, i.e., $[\![\hat{\pi}_i]\!]_0 + [\![\hat{\pi}_\ell]\!]_0 = 0$, gives a general jump condition of

$$\sigma[\![(-\sigma + \nu L)\hat{w}' - f\hat{\zeta}]\!]_0 + \tilde{k}^2\Delta B\, \hat{w}(0) = 0, \tag{A6}$$

where we have used the kinematic condition $\sigma\hat{\eta}(0) = \hat{w}(0)$ from (16). It is possible to use this jump condition to recover all cases examined in the body of the text.

(i) *Inviscid convection*. Setting $\nu = 0$ and using (9) to write $\hat{\zeta} = f\hat{w}'/\sigma$ recovers the jump condition in (23) from (A6). This contains the inviscid, nonrotating jump condition as a special case with $f = 0$.

(ii) *Viscous convection*. For this case, we use $[\![\hat{w}']\!]_0 = [\![\hat{\zeta}]\!]_0 = 0$ and the fact that $[\![L(\hat{w}')]\!]_0 = [\![\hat{w}'']\!]_0$ to recover the jump condition (41) from (A6).

APPENDIX B: HEURISTIC INTERPRETATION

We have largely based our physical interpretations on the interplay of the vorticity, vertical velocity, and displacement fields, using wave interaction theory. However, in this section, we offer a heuristic physical interpretation of the interfacial stabilization mechanism that is not intended to be as formal and quantitative. It describes the stabilization at the stratified interface that comes from including rotation into the inviscid, unbounded setup.

With reference to the sketch in Fig. 8, we see that at an interface growing from a convective instability that is free from rotation, there are overturning circulation cells that are formed [Fig. 8(a)]. These transport mixed layer fluid horizontally away from crests and towards troughs, and are confined to the $\vec{e}^{(k)}$ direction. This can also be thought of as the signature of the alignment of

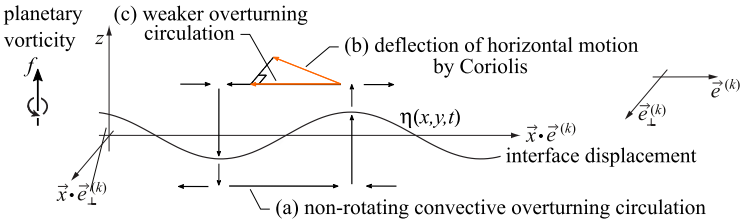

FIG. 8. Sketch of the heuristic interpretation of the interfacial mechanism of stabilization by rotation. Labels (a), (b), and (c) refer to various aspects of the sketch that are referenced in the text, and colors indicate the alterations that are present when rotation is included.

the interfacial vorticity vector with the $\vec{e}_\perp^{(k)}$ direction. However, when rotation is included, these horizontal motions are subject to the Coriolis force that will cause a deflection to the right [for $f > 0$, Fig. 8(b)]. This has the effect of weakening the overturning circulation by creating a component along the interface crests and troughs in the $\vec{e}_\perp^{(k)}$ direction [Fig. 8(c)]. Again, this reflects the fact that the interfacial vorticity vector is misaligned with $\vec{e}_\perp^{(k)}$. This weakening of the overturning circulation reduces the growth of the interface displacement by weakening the vertical velocities associated with the circulation (due to the requirement of satisfying continuity).

Note that in this explanation, we have discussed in terms of velocities and forces, and have neglected to specify the effect of the pressure gradients. This is an advantage of vorticity-based formulations, which eliminate the pressure gradient terms. For this reason, we refer to the explanation as heuristic.

[1] Y. Liang, J. Carpenter, and M.-L. Timmermans, The effect of rotation on double diffusive convection: Perspectives from linear stability analysis, J. Phys. Oceanogr. **51**, 3335 (2021).
[2] S. Chandrasekhar, The instability of a layer of fluid heated below and subject to Coriolis forces, Proc. R. Soc. London A **217**, 306 (1953).
[3] Y. Nakagawa and P. Frenzen, A theoretical and experimental study of cellular convection in rotating fluids, Tellus **7**, 2 (1955).
[4] G. Veronis, Cellular convection with finite amplitude in a rotating fluid, J. Fluid Mech. **5**, 401 (1959).
[5] H. T. Rossby, A study of Benard convection with and without rotation, J. Fluid Mech. **36**, 309 (1969).
[6] F. H. Busse and K. Heikes, Convection in a rotating layer: A simple case of turbulence, Science **208**, 173 (1980).
[7] Y. Hu, R. E. Ecke, and G. Ahlers, Time and Length Scales in Rotating Rayleigh-Bénard Convection, Phys. Rev. Lett. **74**, 5040 (1995).
[8] M. C. Cross and P. C. Hohenberg, Pattern formation outside of equilibrium, Rev. Mod. Phys. **65**, 851 (1993).
[9] A. Pandey, J. D. Scheel, and J. Schumacher, Turbulent superstructures in Rayleigh-Bénard convection, Nat. Commun. **9**, 2118 (2018).
[10] K. Julien, S. Legg, J. McWilliams, and J. Werne, Rapidly rotating turbulent Rayleigh-Bénard convection, J. Fluid Mech. **322**, 243 (1996).
[11] S. Stellmach, M. Lischper, K. Julien, G. Vasil, J. S. Cheng, A. Ribeiro, E. M. King, and J. M. Aurnou, Approaching the Asymptotic Regime of Rapidly Rotating Convection: Boundary Layers versus Interior Dynamics, Phys. Rev. Lett. **113**, 254501 (2014).
[12] V. M. Canuto and M. S. Dubovikov, Two Scaling Regimes for Rotating Rayleigh-Bénard Convection, Phys. Rev. Lett. **80**, 281 (1998).
[13] Y. Liu and R. E. Ecke, Heat Transport Scaling in Turbulent Rayleigh-Bénard Convection: Effects of Rotation and Prandtl Number, Phys. Rev. Lett. **79**, 2257 (1997).

[14] J.-Q. Zhong, R. J. A. M. Stevens, H. J. H. Clercx, R. Verzicco, D. Lohse, and G. Ahlers, Prandtl-, Rayleigh-, and Rossby-Number Dependence of Heat Transport in Turbulent Rotating Rayleigh-Bénard Convection, Phys. Rev. Lett. **102**, 044502 (2009).
[15] E. King, S. Stellmach, and J. Aurnou, Heat transfer by rapidly rotating Rayleigh-Benard convection, J. Fluid Mech. **691**, 568 (2012).
[16] R. J. Stevens, H. J. Clercx, and D. Lohse, Heat transport and flow structure in rotating Rayleigh–Bénard convection, Eur. J. Mech. B Fluids **40**, 41 (2013).
[17] J. Carpenter, T. Sommer, and A. Wüest, Stability of a double-diffusive interface in the diffusive convection regime, J. Phys. Oceanogr. **42**, 840 (2012).
[18] K. A. Baldwin, M. M. Scase, and R. J. A. Hill, The inhibition of the Rayleigh-Taylor instability by rotation, Sci. Rep. **5**, 11706 (2015).
[19] P. Baines, *Topographic Effects in Stratified Flows* (Cambridge University Press, Cambridge, 1995).
[20] W. Smyth and J. Carpenter, *Instability in Geophysical Flows* (Cambridge University Press, Cambridge, 2019)
[21] P. Baines and H. Mitsudera, On the mechanism of shear flow instabilities, J. Fluid Mech. **276**, 327 (1994).
[22] C. Caulfield, Multiple linear instability of layered stratified shear flow, J. Fluid Mech. **258**, 255 (1994).
[23] J. Carpenter, N. Balmforth, and G. Lawrence, Identifying unstable modes in stratified shear layers, Phys. Fluids **22**, 054104 (2010).
[24] E. Heifetz and J. Methven, Relating optimal growth to counterpropagating Rossby waves in shear instability, Phys. Fluids **17**, 064107 (2005).
[25] J. Carpenter, E. Tedford, E. Heifetz, and G. Lawrence, Instability in stratified shear flows: Review of a physical mechanism based on interacting waves, Appl. Mech. Rev. **64**, 060801 (2011).
[26] E. Heifetz, A. Guha, and J. Carpenter, Wave interactions in neutrally stable shear layers: Regular and singular modes, and nonmodal growth, Phys. Fluids **32**, 074106 (2020).
[27] X. Wang, Infinite Prandtl number limit of Rayleigh-Bénard convection, Commun. Pure Appl. Math. **57**, 1265 (2004).
[28] This comes from the definition of horizontal stress of $\tau_{xz} = \rho_0 \nu(\partial u/\partial z + \partial w/\partial x)$ and $\tau_{yz} = \rho_0 \nu(\partial v/\partial z + \partial w/\partial y)$. If the partial derivatives in x and y are taken to τ_{xz} and τ_{yz}, respectively, and they are added together, then the jump condition is derived after using $[\![\hat{w}]\!]_0 = 0$.
[29] S. Chandrasekhar, *Hydrodynamic and Hydromagnetic Stability*, 1st ed. (Dover, Mineola, NY, 1961).
[30] P. Kundu, I. Cohen, and H. Hu, *Fluid Mechanics*, 2nd ed. (Elsevier, New York, 2004).
[31] E. Heifetz, Y. Reuveni, A. Gelfgat, E. Kit, and J. Methven, Counterpropagating Rossby wave perspective on Kelvin Helmholtz instability as a limiting case of a Rayleigh shear layer with zero width, Phys. Fluids **18**, 018101 (2006).
[32] J. Carpenter and A. Guha, Instability of a smooth shear layer through wave interactions, Phys. Fluids **31**, 081701 (2019).
[33] M. Roberts and J. Jacobs, The effects of forced small-wavelength, finite-bandwidth initial perturbations and miscibility on the turbulent Rayleigh-Taylor instability, J. Fluid Mech. **787**, 50 (2016).
[34] E. Heifetz, A. Maor, and A. Guha, On the opposing roles of the Boussinesq and non-Boussinesq baroclinic torques in surface gravity wave propagation, Qtrly. J. R. Meteorolog. Soc. **146**, 1056 (2020).
[35] In our expressions for the vertical velocity at the interface, $\hat{w}(0)$, we always include proportionality to the interfacial vorticity component $\vec{\hat{\gamma}} \cdot \vec{e}_{\perp}^{(k)}$. This quantity serves as a normalization that is needed when comparing different cases (e.g., bounded and unbounded domains).
[36] S. Chandrasekhar, The character of the equilibrium of an incompressible heavy viscous fluid of variable density, Math. Proc. Cambridge Philos. Soc. **51**, 162 (1955).
[37] M. S. Davies Wykes and S. Dalziel, Efficient mixing in stratified flows: Experimental study of a Rayleigh-Taylor unstable interface within an otherwise stable stratification, J. Fluid Mech. **756**, 1027 (2014).
[38] R. Hide, The character of the equilibrium of a heavy, viscous, incompressible, rotating fluid of variable density II: Two special cases, Qtrly. J. Mech. Appl. Math. **9**, 35 (1956).